Available online at www.sciencedirect.com
ScienceDirect
Journal of Power Sources 171 (2007) 747–753
JOURNAL OF POWER SOURCES
www.elsevier.com/locate/jpowsour

Structure and impedance spectroscopy of $La_{0.6}Ca_{0.4}Fe_{0.8}Ni_{0.2}O_{3-\delta}$ thin films grown by pulsed laser deposition

I. Ruiz de Larramendi, N. Ortiz, R. López-Antón [1,2], J.I. Ruiz de Larramendi, T. Rojo *

Departamento de Química Inorgánica, Facultad de Ciencia y Tecnología, Universidad del País Vasco, Apdo. 644, 48080 Bilbao, Spain

Received 20 February 2007; received in revised form 24 May 2007; accepted 9 June 2007
Available online 23 June 2007

Abstract

Polycrystalline samples of $La_{0.6}Ca_{0.4}Fe_{0.8}Ni_{0.2}O_3$ (LCFN) were prepared by the liquid mix process at 600 °C. The structure of the polycrystalline powders was analyzed with X-ray powder diffraction data. The XRD patterns were indexed as the orthoferrite similar to that of $PrFeO_3$ having a single phase orthorhombic perovskite structure (*Pbnm*).

LCFN films have been deposited on yttria-stabilized zirconia (YSZ) single crystal and polycrystalline substrates at 700 °C by pulsed laser deposition (PLD) for application to thin film solid oxide fuel cell cathodes. The structure of the films was analyzed by X-ray diffraction (XRD), scanning electron microscopy (SEM) and atomic force microscopy (AFM). Both films are polycrystalline with a marked texture and present pyramidal grains in the surface with different size distribution. Electrochemical impedance spectroscopy (EIS) measurements of LCFN/YSZ single crystal/LCFN and LCFN/polycrystalline YSZ/LCFN test cells were conducted. The obtained ASR values at 850 °C for the single crystal and polycrystalline YSZ cell tests were 1.84 and 1.59 Ω cm^2, respectively.

Keywords: SOFC; Cathodes; Perovskite; Pulsed laser deposition; Electrochemical impedance spectroscopy

1. Introduction

Solid oxide fuel cells (SOFC) are considered a promise device to convert energy that exhibits main advantages such as high efficiency and low environmental impact. The energy conversion is direct without any intermediate phase. The most common materials for the SOFC are oxide ion conducting yttria-stabilized zirconia (YSZ) for the electrolyte, strontium-doped lanthanum magnanite (LSM) for the cathode, nickel/YSZ cerment for the anode, and doped lanthanum chromite or refractory metals as interconnect materials.

The traditional SOFC operated at high temperature up to 1000 °C presents some problems related to the cost of the materials and fabrication. Therefore, an important research is to get lower cost components for operation temperatures under 800 °C. Accordingly, intermediate temperature solid oxide fuel cells (IT-SOFC), operating in that range of temperatures, have attracted much attention in recent years [1].

One of the vital SOFC components is the cathode. In particular, perovskite materials are well known for their more than adequate characteristics as solid oxide fuel cell (SOFC) cathode materials. Sr-doped $LaMnO_3$ (LSM) has been widely studied for decades as a cathode material, primarily due to its relatively high electrocatalytic activity for O_2 reduction and good thermal and chemical compatibility with Y_2O_3-stabilized ZrO_2 (YSZ) electrolyte [2]. Chemical reactivity between LSM and YSZ leads to the formation of the pyrochlore, $La_2Zr_2O_7$ (LZO). The formation of LZO reduces cathode performance because it has significantly lower conductivity than LSM or YSZ at fuel cell operating temperatures [3]. An additional problem of LSM is its high thermal expansion coefficient, which could be solved by substituting some of the Mn ions by Ni or Fe ions. It is also known that $LaNiO_3$ has a very high electronic conductivity at room temperature. However, $LaNiO_3$ is unstable above 850 °C, where it decomposes to La_2NiO_4 and NiO. When Fe is used as substitution, it was shown that this material is stable at high temperature. When the Fe fraction is

* Corresponding author. Tel.: +34 94 6012458; fax: +34 94 6013500.
E-mail address: teo.rojo@ehu.es (T. Rojo).
[1] Current address: Instituto de Ciencia de Materiales de Aragón, CSIC-Universidad de Zaragoza, C/Pedro Cerbuna 12, 50009 Zaragoza, Spain.
[2] Current address: ISIS Neutron and Muon Facility, Rutherford Appleton Laboratory, Chilton, Didcot, Oxfordshire OX11 0QX, UK.

0378-7753/$ – see front matter © 2007 Elsevier B.V. All rights reserved.
doi:10.1016/j.jpowsour.2007.06.062

higher than 0.5, the material has a high electronic conductivity (e.g., $La_{0.6}Sr_{0.4}Ni_{0.2}Fe_{0.8}O_3$ 435 S cm^{-1} at 800 °C) [4,5]. Calcium is another effective doping-element at the A-site of ABO_3, with lower cost. Moreover, calcium could be a good candidate because of the similarity of its ionic radius with La^{3+} which could give a higher stability than the strontium substitution [6]. Hence, $La_{0.6}Ca_{0.4}Fe_{0.8}Ni_{0.2}O_3$ (LCFN in the following) seems a very well-suited material as cathode for these SOFC.

On the other hand, pulsed laser deposition (PLD) has been recently used to fabricate La–Sr–Co–O thin films for application to SOFC [7–14], as using integrated oxide thin films for fuel cell design can reduce the size and cost of cells. Due to its high chemical reactivity with yttria-stabilized zirconia at high temperature [15], doped lanthanum cobaltite cannot be used as a cathode in high temperature SOFCs. Another important factor is the porosity in such a cathode, as it could help increase gas transport to the reaction sites at the surface of the electrolyte (usually yttria-stabilized zirconia—YSZ). Therefore, we have obtained several $La_{0.6}Ca_{0.4}Fe_{0.8}Ni_{0.2}O_3$ (LCFN) thin films by PLD and studied the influence of the substrate on the crystallinity and porosity of the samples, looking for thin films with high crystallinity and porosity. LCFN films have been deposited on single crystal and polycrystalline YSZ substrates by PLD. X-ray diffraction (XRD), atomic force microscopy (AFM), scanning electron microscopy (SEM) and electrical conductivity measurements have been performed. The electrical conductivity data have also been compared with those of LSM thin films obtained by PLD and with test cells made painting LCFN material on both sides of a YSZ single crystal.

2. Experimental

2.1. Sample preparation

Powders of $La_{0.6}Ca_{0.4}Fe_{0.8}Ni_{0.2}O_{3-\delta}$ perovskite were prepared by the liquid mix process. Appropriate amounts of the nitrate salts [$La(NO_3)_3{\cdot}6H_2O$; $Ca(NO_3)_2{\cdot}H_2O$; $Fe(NO_3)_3{\cdot}9H_2O$; $Ni(NO_3)_2{\cdot}6H_2O$] and citric acid were dissolved in distilled water and later the suitable volume of ethylene glycol was added. The resulting solution was shaked and heated in a heating plate until the formation of a gel. After that, the gel which was already treated in a sand bath, was calcined at 600 °C in a oven for 12 h with a 1° min^{-1} rate. The resulting powders were pressed into pellets and calcined again at 1200 °C for 10 h.

Using these sintered pellets as targets, LCFN films have been deposited on single crystal (1 0 0) and polycrystalline YSZ substrates by PLD. The samples were deposited using a LAMBDA PHYSIC Compex 102 KrF excimer laser (248 nm, 150 mJ pulse^{-1}) at a frequency of 15 Hz. The target was placed in a rotating target holder in a vacuum chamber with an initial pressure of 2×10^{-6} mbar. Y-doped zirconia (YSZ), in single crystal and polycrystalline form, was used as substrate. The substrates were mounted on a heater and the films were deposited at a substrate temperature of 700 °C, taking into account the existing literature [7–10] and our previous experience in PLD in similar samples [16]. The temperature of the substrate is one of the main parameter affecting atomic surface mobility during the deposition process. Oxygen gas was flowed into the chamber in a constant flux during deposition, keeping a pressure of 0.3 mbar. Deposition time was 120 min. LSM thin films have been prepared using a commercial powder (Praxair) in the same deposition conditions so as to compare their transport properties with the LCFN samples.

2.2. Characterization of the thin films

The powders and films were characterized by X-ray powder diffraction data, collected using a Philips PW1710 and Philips X'Pert-MPD (Bragg-Brentano geometry) diffractometers, with Cu K_α radiation, and fitted using the FULLPROF program [17]. The atomic force microscopy (AFM) measurements were performed using a commercial scanning probe microscope (Nanotec DSP classic). The microstructure of the obtained films was observed by scanning electron microscopy (SEM) using a JEOL JSM-6400 microscope at 20 kV accelerating voltage.

2.3. Electrochemical measurements

Testing cells of LCFN/YSZ/LCFN were made by deposition of $La_{0.6}Ca_{0.4}Fe_{0.8}Ni_{0.2}O_{3-\delta}$ on the two sides of a YSZ wafer, in order to measure their transport properties by electrochemical impedance spectroscopy (EIS) and to compare their properties with the already prepared cells of LCFN/YSZ/LCFN made by painting both sides of the electrolyte with a LCFN paste. The thickness of the substrates was $e \approx 0.50$ mm, whereas that of the films was about 3 μm, and the surface area about 1 cm^2. Electrical contacts were platinum grids pressed on both sides of the sample in order to obtain a symmetrical cell. In Fig. 1, a schematic drawing of the symmetrical testing cell is shown.

Electrochemical impedance spectroscopy (EIS) measurements of LCFN/YSZ/LCFN test cells were conducted using a Solartron 1260 Impedance Analyzer. The frequency range was 10^{-2} to 10^6 Hz with a signal amplitude of 50 mV. All these electrochemical experiments were performed at equilibrium from room temperature up to 850 °C, under zero dc current intensity and under air over a cycle of heating and cooling. Impedance diagrams were analyzed and fitted using the Zview software. Resistance, capacitance and the values from the fitting of each semicircle in the EIS measurements were obtained by least-square refinement.

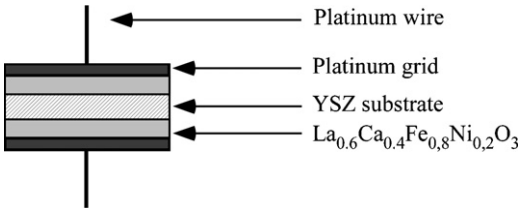

Fig. 1. Schematic drawing of the symmetrical testing cell.

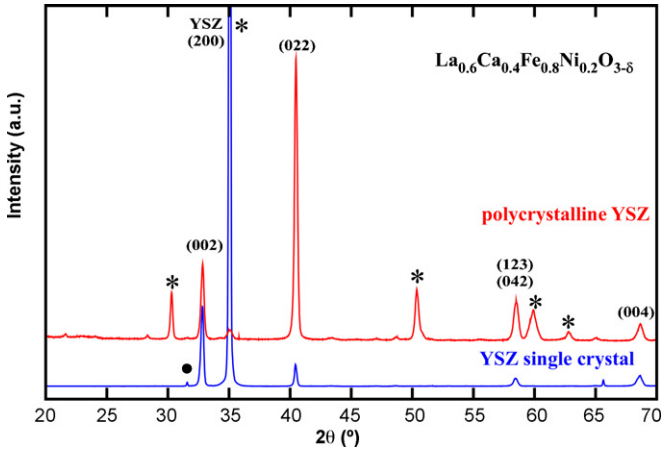

Fig. 2. XRD patterns of $La_{0.6}Ca_{0.4}Fe_{0.8}Ni_{0.2}O_{3-\delta}$ films obtained at 700 °C on both substrates: (a) (1 0 0) YSZ single crystal and (b) YSZ polycrystalline (*, substrate reflections; ●, Cu K_β).

3. Results and discussion

3.1. Characterization of the thin films

The XRD diffractograms of the as-deposited thin films are shown in Fig. 2 whereas in Fig. 3 are shown the diffraction profile of the target and the fitted profiles of the thin film deposited at 700 °C on both substrates. The reflections corresponding to the LCFN crystalline phase are observed in the as-deposited samples, together with very strong peaks due to the single crystal and polycrystalline YSZ substrates (e.g., the intense peak appearing at about 35 °(θ) appearing in the film deposited on the single crystal substrate, corresponding to the (2 0 0) reflection of the substrate). In fact, this peak is so intense given the crystallinity of the substrate that even its corresponding Cu K_β reflection is observed, despite the existence of a monochromator). A polycrystalline growth is found in both films. This was expected for the deposition on the polycrystalline substrate but the conditions in which the deposit has been performed on the single crystal substrate are well suited for an epitaxial growth (single crystal substrate, high temperature, etc.). However, due to the great difference between the structures of the substrate (fluorite-type, *Fm*3*m* S.G.) and the target (perovskite-type *Pbnm* S.G.), a polycrystalline growth is also found.

It can be appreciated in Fig. 3 that in both cases an important texture is observed. In particular, this texture is in the preferential direction of the substrate (hence, the preferential direction is (2 0 0) in the film deposited on the single crystal substrate, whereas in the sample deposited on the polycrystalline substrate the preferential direction is (2 2 0)). This trend was also observed in $Pr_{0.8}Sr_{0.2}Fe_{0.8}Ni_{0.2}O_{3-\delta}$ films deposited on YSZ single crystal substrates [16]. In addition of the role of the substrate, the partial oxygen pressure cannot only affect the oxygen stoichiometry but also the texture and orientation of this kind of films [9]. The peaks of the film are quite wider than those of the target, pointing out a smaller particle size and likely a certain stress in the film due to the commented structural difference between the substrate and the film.

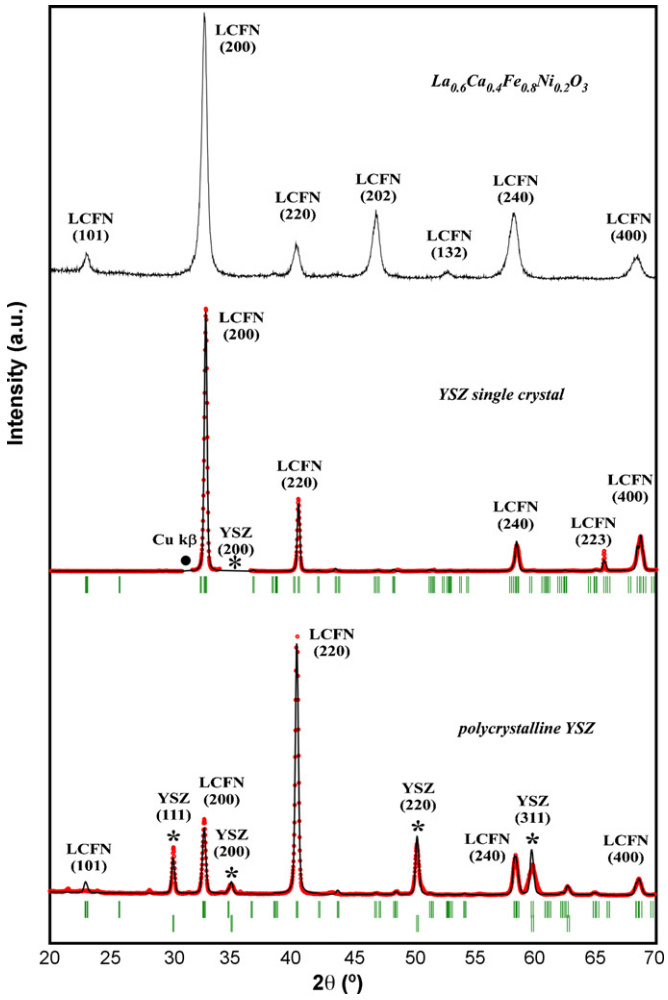

Fig. 3. Diffraction profiles of the $La_{0.6}Ca_{0.4}Fe_{0.8}Ni_{0.2}O_{3-\delta}$ phase: of the target (upper side) and experimental (squares), fitted (line) and difference between them (lower line) profiles of the thin film deposited at 700 °C on the single crystal (middle side) and on the polycrystalline YSZ (lower side) substrates.

The AFM micrographs of the films are shown in Fig. 4 whereas Fig. 5 shows SEM images taken on the surface and on the cross-section of the films. In both AFM and SEM micrographs pyramidal grains are found, which have been also observed by other groups in PLD thin films of perovskite oxides [18,19]. In both samples there is a size distribution of the grains but in the case of the one deposited on a polycrystalline substrate, there are more small grains than in the other one. The cross-section images show a columnar growth of the films, although the thin film deposited on the polycrystalline substrate exhibit narrower columns, which agrees well with the bigger quantity of small grain observed in its corresponding surface micrograph. Therefore, given its narrower columns and its corresponding size distribution, the film deposited on polycrystalline YSZ is more dense (with higher specific surface area), which could greatly affect its conductive properties of the sample, as it will be shown.

In the images of the cross-section is observed that both films have a thickness of about 3 μm, being slightly lower in the case of the sample deposited on a single crystal.

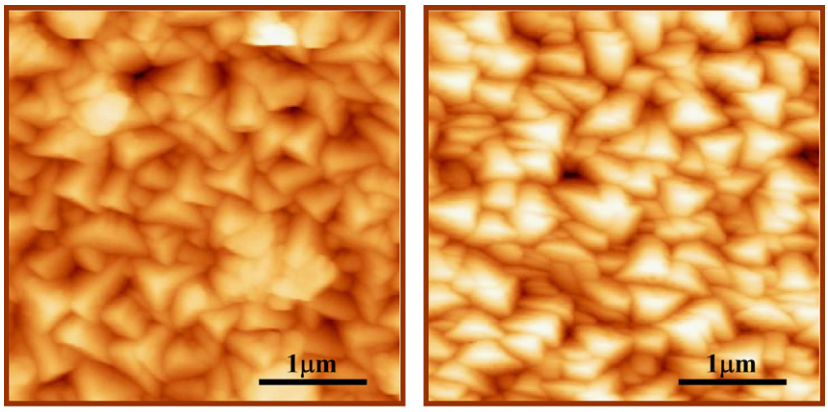

Fig. 4. AFM micrographs of the films deposited at 700 °C on: (a) single crystal and (b) polycrystalline YSZ substrates. The frame size of the images is 3.5 μm × 3.5 μm.

3.2. Electrochemical measurements

In Fig. 6 Nyquist plot of LCFN/polycrystalline YSZ/LCFN cell measured at 300 °C, in air, is shown. In this figure there are detailed the different processes that can be seen at low temperatures, appreciating the appearance of three depressed semicircles. In both substrates, at high frequencies the semicircle appears due to the bulk of the compound, with a value of capacitance of 4.61×10^{-12} and 4.36×10^{-12} F for the single crystal and the polycrystalline substrates, respectively. These values agree with the obtained ones of the bibliography [20]. The following semicircle that is observed at not so high frequencies is due to the grain boundary of the substrate, with a capacitance of $3{,}36 \times 10^{-9}$ F. In the case of the single crystal, this contribution, obviously, is not observed. Later, at medium and lower frequencies the semicircles due to the different processes that take place in the electrode (interface processes, electrode reactions, etc.) are found, but these contributions are better studied at high temperatures.

Typical electrochemical impedance spectra for LCFN/YSZ/LCFN cells, using both different substrates, are reported in the Nyquist plan at 450 °C (Fig. 7) and at 850 °C (Fig. 8). At 450 °C, a series of depressed semicircles can be appreciated for both substrates. In the case of the single crystal,

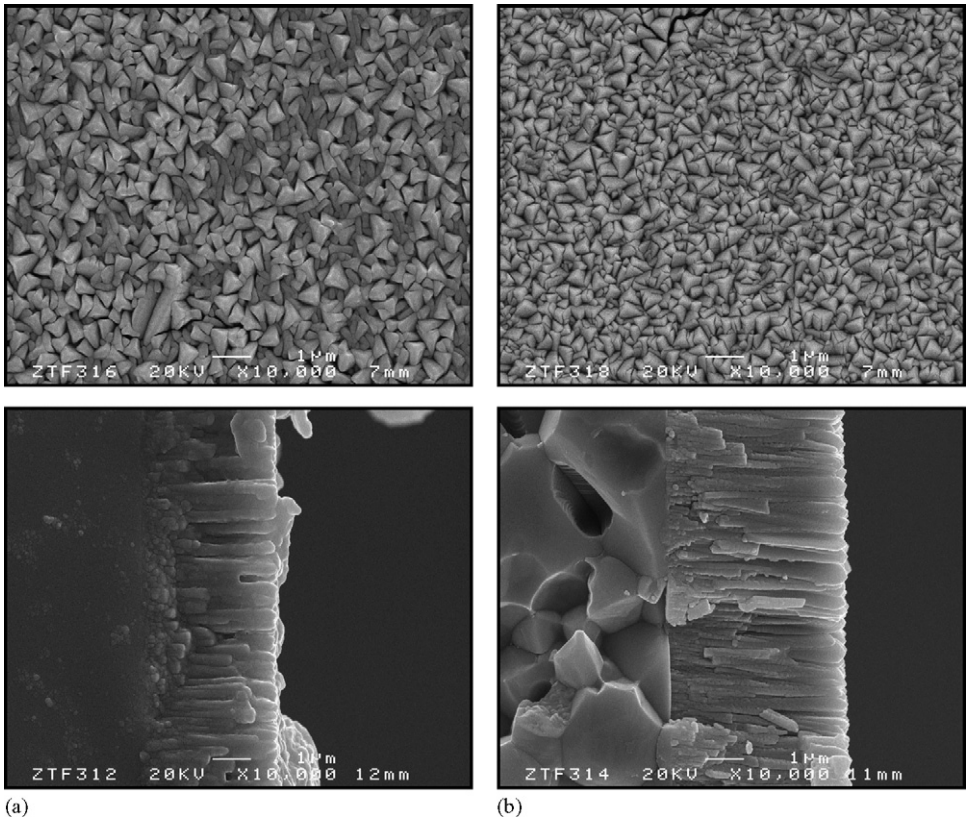

Fig. 5. SEM images of the surface and cross-section of the films on: (a) single crystal and (b) polycrystalline YSZ substrates.

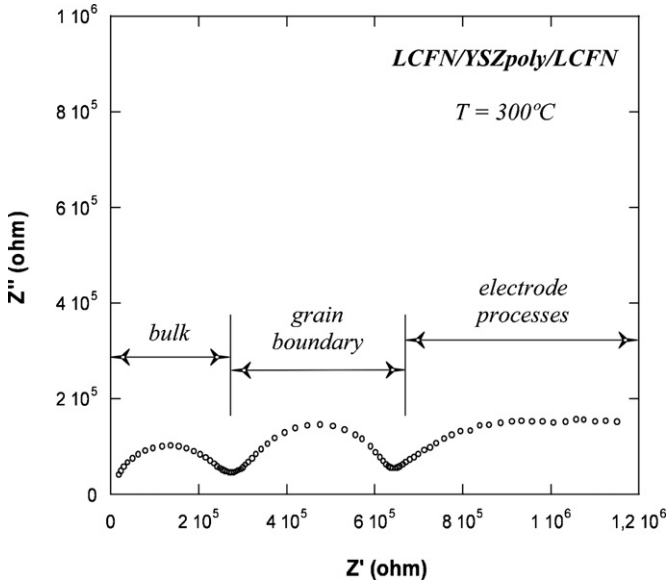

Fig. 6. Typical impedance diagrams obtained with LCFN/YSZ (polycrystalline) half cells, under air, at 300 °C.

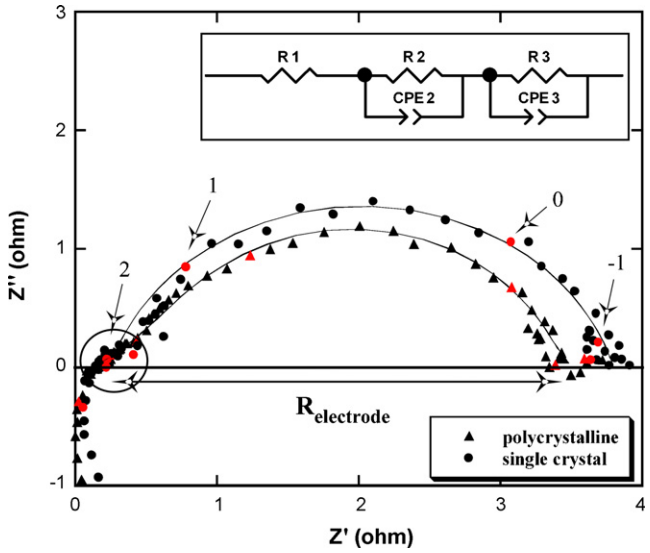

Fig. 8. Typical impedance diagrams obtained with LCFN/YSZ half cells, under air, at 850 °C (inset: equivalent circuit used for fitting data). Circle indicates the additional small arc. The impedance data are plotted after electrolyte ohmic drop correction. The numbers by data points are frequency logarithms.

the first semicircle (HF) is the correspondent to the bulk of the electrolyte, whereas in case of the polycrystalline substrate the correspondent to the grain boundary is also observed. At minor frequencies (MF and LF), the appearance of the contribution of the processes in the electrode is shown, being minor in importance in the case of the polycrystalline substrate. At 850 °C only the processes of the cathode are distinguished. In both cases the resistance associated with the above-mentioned processes is very small, being slightly minor in the case of the polycrystalline substrate. The polycrystalline YSZ is known to show lower activation energies of the involved processes than the single crystal, which favors hopping of the oxygen vacancies, improving ionic conduction [21].

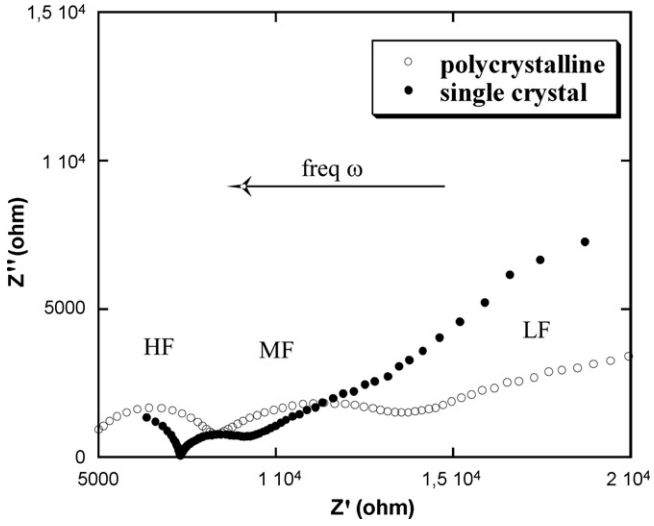

Fig. 7. Typical impedance diagrams obtained with LCFN/YSZ half cells, under air, at 450 °C (HF: high frequencies; MF: medium frequencies; LF: low frequencies).

In Fig. 8 the fit obtained for both substrates at 850 °C is shown. The equivalent circuit that best fits the data is shown as inset in this figure where R1, R2 and R3 are ohmic resistance, diffusion in the perovskite, and dissociative adsorption on the electrode surface, respectively [11]. The R2 and R3 have constant phase elements (CPE) in parallel to simulate the distribution of relaxation time in the real system. Both semicircles are overlapped, which difficulties the analysis of the results obtained for each process. At high temperatures, an additional arc appeared (indicated by a circle in Fig. 8) which, according to several authors, is independent of temperature [22]. Zhu et al. found that the low-frequency arc is therefore ascribed to gas diffusion.

In Fig. 9, the Arrhenius plot of capacitances of the different contributions is shown for both used substrates. A study was carried out according to the methodology proposed by Schouler et al. [20], where the thermal evolution of the relaxation frequencies, f_r, is independent from the geometric characteristics of the sample, which enabled us to associate the different contributions to their respective processes.

At high frequencies (HF) the different electrolyte contributions are appreciated, being observable only at low temperatures. The contributions at higher frequencies are due to the contribution of the bulk, whereas the processes produced in the grain boundary are indicated as g.b. The capacitances values assigned to the YSZ polycrystalline electrolyte bulk and grain boundary processes are 10^{-12} and 10^{-9} F cm^{-3}, respectively. On the other hand, at lower frequencies two different contributions can be seen for the electrodic processes which are associated with mixed ionic and electronic conductors (MIEC) behavior [23]. The oxygen reduction mechanism on porous MIEC electrodes may involve several processes such as charge transfer at the current collector/electrode interface and electrode/electrolyte interfaces, oxygen exchange at the electrode surface, bulk and surface diffusion of oxygen species and gas phase diffusion. To

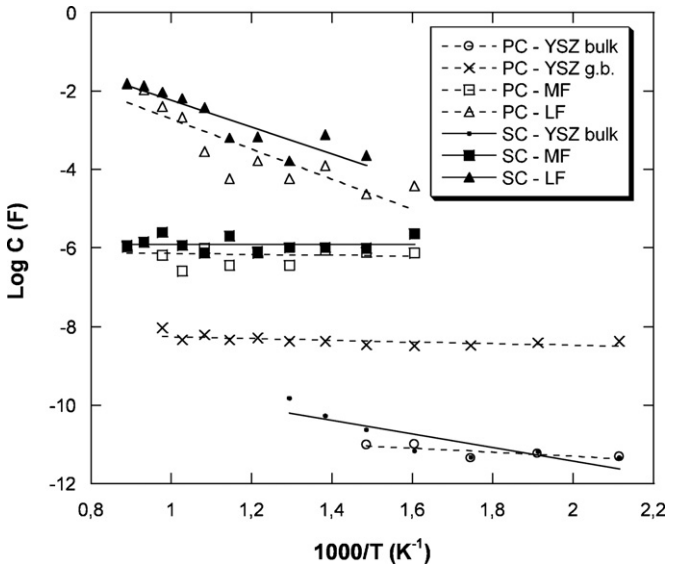

Fig. 9. Arrhenius plots of capacitances (C) for the LCFN/YSZ/LCFN cells under air and zero dc conditions (PC: polycrystalline YSZ; SC: single crystal YSZ; MF: medium frequencies; LF: low frequencies).

be able to assign every contribution with its respective semicircle, it will be necessary to realize measurements in different oxygen partial pressures, so that study will be carried out in further works under way.

The area-specific resistance (ASR) is deduced from the relation: $ASR = R_{electrode} \times SurfaceArea/2$. The Arrhenius plots of the ASR values for LCFN/YSZ single crystal/LCFN and LCFN/polycrystalline YSZ/LCFN half cells are given in Fig. 10.

In both cases, ASR values remain over 1 $\Omega\,cm^2$. The sample deposited on polycrystalline YSZ presents a lower ASR value, 1.59 $\Omega\,cm^2$ at 850 °C, than the one obtained for the phase deposited onto YSZ single crystal, 1.84 $\Omega\,cm^2$. These values are fairly smaller than the obtained ones on having painted the material LCFN on YSZ's pellet, where an ASR of 85.87 $\Omega\,cm^2$ is obtained [24]. The obtained values for LCFN thin films are

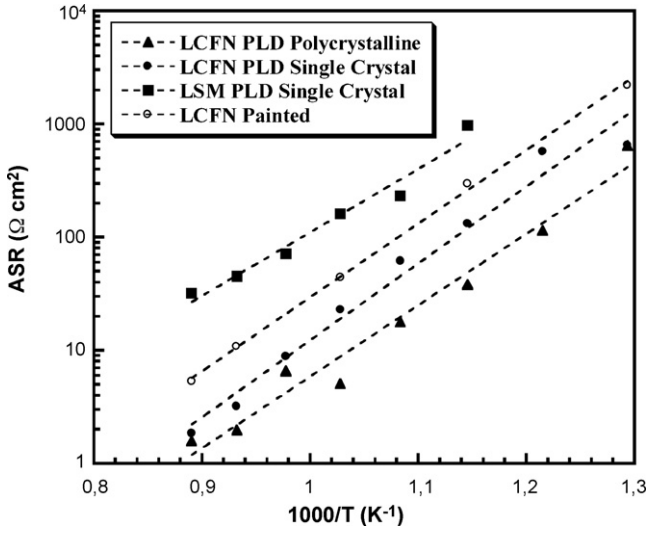

Fig. 10. Arrhenius plots of ASR for LCFN electrode with two different substrates.

quite lower than those corresponding to LSM thin films fabricated by PLD (ASR = 32.10 $\Omega\,cm^2$ at 850 °C), which agrees well with the literature [25]. Greater resistance values are found for the test cells obtained by painting the LCFN material on the single crystal (ASR = 5.33 $\Omega\,cm^2$ at 850 °C). However, we should take into account that the conduction processes involved are different in both cases: the painted films are porous, giving place to three phase boundary (TPB) conduction, where the reactive gas meets the electrode and the electrolyte phases, whereas for the PLD thin films, being dense, there is no direct contact between the cathode, electrolyte and gas (hence no TPB conduction exists). Therefore, in this case the oxygen reduction reaction occurs anywhere on the cathode surface, forming oxide anions which the diffuse into the bulk of the electrode material towards the electrolyte.

4. Conclusions

Polycrystalline thin films of $La_{0.6}Ca_{0.4}Fe_{0.8}Ni_{0.2}O_3$ have been deposited on two different substrates: (1 0 0) YSZ single crystal and polycrystalline YSZ, at 700 °C. Both films are polycrystalline with a marked texture, favoring the preferential direction of the substrate. The examination of the cross-section structure of the films by SEM revealed a dense ordered columnar structure, with narrower columns for the sample deposited on the polycrystalline substrate. On the surface pyramidal grains, with a certain size distribution, are visible. The film thickness is about 3 μm, being slightly lower in the case of the single crystal substrate. The electrochemical performance of the LCFN material on (1 0 0) YSZ single crystal and polycrystalline YSZ substrates as electrolyte was made. This electrochemical measurements showed a better performance for the polycrystalline electrolyte with an ASR value at 850 °C of 1.59 $\Omega\,cm^2$ measured in a two-electrode configuration using symmetrical cells.

Acknowledgements

This work has been partially financed by the Spanish CiCyT under project MAT2004-02425. I. Ruiz de Larramendi thanks the Eusko Jaurlaritza/Gobierno Vasco for her predoctoral fellowship and R.L.A. thanks the Spanish CiCyT for funding his research activities as postdoc within the Project MAT2004-02425.

References

[1] W. Wang, S.P. Jiang, Solid State Ionics 177 (2006) 1361.
[2] C. Chervin, R.S. Glass, S.M. Kauzlarich, Solid State Ionics 176 (2005) 17.
[3] G. Zhu, X. Fang, C. Xia, X. Liu, Ceram. Int. 31 (2005) 116.
[4] R. Chiba, F. Yoshimura, Y. Sakurai, Solid State Ionics 152–153 (2002) 575.
[5] R. Chiba, F. Yoshimura, Y. Sakurai, Solid State Ionics 124 (1999) 281.
[6] P. Ciambelli, S. Cimino, L. Lisi, M. Faticanti, G. Minelli, I. Pettiti, P. Porta, Appl. Catal. B: Environ. 33 (2001) 194.
[7] X. Chen, N.J. Wu, A. Ignatiev, J. Eur. Ceram. Soc. 19 (1999) 819.
[8] X. Chen, N.J. Wu, D.L. Ritums, A. Ignatiev, Thin Solid Films 342 (1999) 61.
[9] X. Chen, S. Wang, Y.L. Yang, L. Smith, N.J. Wu, B.-I. Kim, S.S. Perry, A.J. Jacobson, A. Ignatiev, Solid State Ionics 146 (3–4) (2002) 405.
[10] X. Chen, N.J. Wu, L. Smith, A. Ignatiev, Appl. Phys. Lett. 84 (2004) 2700.

[11] N. Imanishi, T. Matsumura, Y. Sumiya, K. Yoshimura, A. Hirano, Y. Takeda, D. Mori, R. Kanno, Solid State Ionics 174 (2004) 245.
[12] D. Mori, H. Oka, Y. Suzuki, N. Sonoyama, A. Yamada, R. Kanno, Y. Sumiya, N. Imanishi, Y. Takeda, Solid State Ionics 177 (2006) 535.
[13] N. Imanishi, Y. Sumiya, K. Yoshimura, T. Matsumura, A. Hirano, Y. Takeda, D. Mori, R. Kanno, Solid State Ionics 177 (2006) 749.
[14] L.R. Pederson, P. Singh, X.-D. Zhou, Vacuum 80 (2006) 1066.
[15] F.M. Figueiredo, J.A. Labrincha, J.R. Frade, F.M.B. Marques, Solid State Ionics 101 (1997) 343.
[16] I.R. de Larramendi, R.L. Antón, J.I.R. de Larramendi, S. Baliteau, F. Mauvy, J.C. Grenier, T. Rojo, J. Power Sources 169 (1) (2007) 35.
[17] J. Rodríguez-Carvajal, FULLPROF Program, Grenoble, Illinois, 1994.
[18] N. Scarisoreanu, F. Craciun, G. Dinescu, P. Verardi, M. Dinescu, Thin Solid Films 453–454 (2004) 399.
[19] W. Wu, K.H. Wong, C.L. Choy, J. Phys. D: Appl. Phys. 32 (1999) L57.
[20] E.J.L. Schouler, N. Mesbahi, G. Vitter, Solid State Ionics 9–10 (1983) 989.
[21] D. Vladikova, J.A. Kilner, S.J. Skinner, G. Raikova, Z. Stoynov, Electrochim. Acta 51 (2006) 1611.
[22] G. Zhu, X. Fang, C. Xia, X. Liu, Ceram. Int. 31 (2005) 115–119.
[23] F. Mauvy, C. Lalanne, J.M. Bassat, J.C. Grenier, H. Zhao, L. Huo, P. Stevens, J. Electrochem. Soc. 153 (8) (2006) A1547.
[24] I. Ruiz de Larramendi, N. Ortiz, J.I. Ruiz de Larramendi, T. Rojo, Electrochemical Society Transactions-Solid Oxide Fuel Cells 7 (1) (2007) 1157–1164.
[25] A. Endo, M. Ihara, H. Komiyama, K. Yamada, Solid State Ionics 86-88 (1996) 1191.